Microwave-Assisted Preparation of Mo_2C/CNTs Nanocomposites as Efficient Electrocatalyst Supports for Oxygen Reduction Reaction

Min Pang,[†] Chuang Li,[†] Ling Ding,[†] Jian Zhang,[‡] Dangsheng Su,[‡] Wenzhen Li,[§] and Changhai Liang*,[†]

State Key Laboratory of Fine Chemicals and Key Laboratory for Micro/Nano Technology and System of Liaoning Province, Dalian University of Technology, China, Department of Inorganic Chemistry, Fritz Haber Institute of the Max Planck Society, Germany, and Department of Chemical Engineering, Michigan Technological University, Houghton, Michigan 49931

Nanostructured Mo_2C/CNTs composites have been synthesized by using a novel methodology of microwave-assisted thermolytic molecular precursor with $Mo(CO)_6$ as single source precursor. Pt electrocatalysts supported on the Mo_2C/CNTs composites were prepared by using the modified ethylene glycol method. The resulting Mo_2C/CNTs and Pt−Mo_2C/CNTs were characterized by inductively coupled plasma-optical emission spectroscopy, thermogravimetric analysis, X-ray diffraction, transmission electron microscopy, and energy-dispersive X-ray spectroscopy. The rotating disk electrode experiments were used to measure electrocatalytic activity for oxygen reduction reaction. The results showed highly dispersed sphere-like Mo_2C and Pt particles with 3−6 nm can be prepared upon CNTs by the above-mentioned methods. The formation process of Mo_2C includes the following steps: decomposition of $Mo(CO)_6$ precursor to the metallic Mo and CO, CO dismutation reaction, formation of the MoO_xC_y by the metallic Mo and CO, the MoO_xC_y carburization to Mo_2C, and further carburization of Mo_2C to Mo_3C_2. The Pt−Mo_2C/CNTs sample gave higher electrochemical surface area and activity for oxygen reduction reaction with a more positive onset potential in acid solution than those of Pt/CNTs under the same condition, which was attributed to the synergistic effect among Pt, Mo_2C, and CNTs. The findings indicate that Mo_2C is an inexpensive and promising alternative to precious metal and worthy of further exploring for other applications in catalysis.

1. Introduction

Proton exchange membrane fuel cells (PEMFCs), including hydrogen fuel cell and direct alcohol fuel cell, have drawn a great deal of attention as alternative power sources for vehicles and for stationary and portable application due to their high energy conversion efficiency, low reaction temperature, and zero emission of environmental pollutants.[1,2] High cost, low activity, and poor durability are still major barriers to the commercialization of PEMFCs, although lots of advances have been made within the past few decades.[3–5] Developing active, robust, and low cost electrocatalysts has been a longstanding research in PEMFCs.

Slow electrode kinetics at the cathode for oxygen reduction reaction (ORR) is considered as one of the major problems in PEMFCs. To increase the activity of ORR and decrease the catalysts cost or Pt loading, one strategy is to explore the novel support materials because they play an important role in the dispersion of Pt nanoparticles and facilitate the transportation of reactants/products, which directly improve the catalytic activity and stability of catalysts.[6–9] Transition metal carbides as electrocatalysts or their supports had an important promotion effect for ORR in PEMFCs, due to their interactions with Pt and being reactive toward the hydrogen peroxide intermediate.[10–12] Transition metal carbides could withstand high temperature, resist poisoning, have good electrical conductivity, maintain stability in acidic solutions, and could efficiently prevent Pt from falling off the support.[13,14] However, preparation of nanostructured carbides with monodispersed particles is very difficult by the conventional methods, which have been inherited from the metallurgical industry at high temperature and are energy-intensive. Although several preparative methods have been developed, including pyrolysis of metal complexes,[15–17] alkaline reduction,[18,19] temperature-programmed reduction,[20,21] carbothermal hydrogen reduction,[22–24] and sonochemical synthesis,[25–27] the controlled synthesis of nanostructured carbides with monodispersed particles still remains a big challenge for their applications in catalysis.

Microwave techniques have been successfully used in organic and inorganic syntheses and have been proven to be more environmental friendly, which require less energy than conventional processes.[28,29] Recently, tungsten and molybdenum carbides from carbon and metal oxides or metals have been synthesized by microwave processing in tens of seconds.[30–32] However, the carbides exist as blocklike irregular crystallites with grain sizes typically ranging from 5 to 10 μm, and the morphology and grain sizes cannot be controlled. Tungsten and molybdenum carbides were also prepared either through fluidization of metal and carbon black powders with Ar gas or from reaction between metal powders and fluidizing ethylene gas by microwave-assisted synthesis.[33] We have developed a method to prepare nanostructured WC_x by the microwave-assisted thermolytic molecular precursor method, which was powerful for generating highly dispersed and uniformly supported catalytic materials in a controlled and reproducible manner,[34,35] and found nanostructured tungsten carbide is an inexpensive and promising alternative to the noble metal catalysts in hydrazine decomposition and direct methanol fuel cells.[36,37] We had also used carbon nanotubes (CNTs) as electrocatalyst supports for direct methanol fuel cell and found the enhancement effect of CNTs on the electrocatalytic activity

* To whom correspondence should be addressed. Tel.: 86 411 39608806. Fax: 86 411 39893991. E-mail: changhai@dlut.edu.cn.
[†] Dalian University of Technology.
[‡] Fritz Haber Institute of the Max Planck Society.
[§] Michigan Technological University.

10.1021/ie901741c
Published on Web 03/26/2010

of ORR.[38–40] Herein, we report, for the first time, the rapid synthesis of CNTs supported molybdenum carbide nanoparticles by the thermolytic molecular precursor method under microwave irradiation. The formation mechanism of molybdenum carbide was also studied through thermolytic process. The resulting Mo_2C/CNTs nanocomposite support has much higher electrocatalytic activity for ORR than CNTs under the same conditions.

2. Experimental Section

CNTs (Shenzhen Nanotech Port Co. Ltd.) were synthesized by CH_4 decomposition over a nickel-based catalyst, and then the catalyst was removed by dissolution typically in aqueous solution of HNO_3. The CNTs were not further preoxidized prior to use. Typically, 0.1 g of CNTs and 0.055 g of molybdenum hexacarbonyl (Johnson Matthey) were put in an agate mortar, and mixed for 15 min. The completely homogeneous precursor mixture was put in a quartz-tube reactor with inner diameter of about 10 mm and fluidized with a flow rate of 30 mL/min argon for 2 h at room temperature to remove oxygen in the reactor and keep the reaction under the inert atmosphere. Next, the reactor was placed in a domestic microwave oven operating at 2.45 GHz with a power of 800 W. Finally, the resulting products were cooled to room temperature under argon. The microwave irradiation time varied from 1 to 15 min to investigate the formation mechanism.

Pt−Mo_2C/CNTs electrocatalysts with 20 wt % Pt loading were prepared by a modified ethylene glycol method. A certain amount of dihydrogen hexachloroplatinic acid was dissolved in ethylene glycol. The pH value was adjusted to 12 by the addition of NaOH in ethylene glycol. After the solution was heated under reflux to 160 °C for 1.5 h, the as-prepared Mo_2C/CNTs were added and sonicated for 5 min for homogeneous dispersion. The pH value was slowly brought down to 2 by the dropwise addition of concentrated HCl. Next, the mixture was heated under reflux to 110 °C and kept for 1.5 h. The whole process was conducted under flowing argon. After being cooled to room temperature, washed many times with deionized water to remove Na^+ and Cl^-, and dried, the Pt−Mo_2C/CNTs sample was obtained. For comparison, Pt/CNTs sample with the same Pt loading was also prepared by the same method.

The Pt content was determined by inductively coupled plasma-optical emission spectroscopy (ICP-OES). The samples were treated with sodium peroxide solution and then nitric acid solution, and the solution was filtered and analyzed by ICP-OES. Thermogravimetric (TG) experiments were also performed in Mettler Toledo TGA/SDTA851e thermogravimetry. The samples were placed in the atmosphere of air and heated at 10 °C/min to the final temperature of 800 °C. X-ray diffraction (XRD) analysis of the samples was carried out using a Rigaku D/Max-RB diffractometer with Cu Kα monochromatized radiation source (λ = 1.54178 Å), operated at 40 kV and 100 mA. Transmission electron microscopy (TEM) was performed using a Philips CM200 FEG transmission electron microscope (accelerating voltage 200 kV) using high-resolution imaging and energy-dispersive X-ray spectroscopy (EDX). The composition distribution analysis with a resolution of a few nanometers was performed in the STEM mode in combination with energy dispersive X-ray spectroscopy (EDX) using a DX4 analyzer system (EDAX) in the same microscope.

A CHI 6DOC potentiostat/galvanostat was used for the electrochemical measurements in a three-electrode electrochemical cell. A rotating disk electrode with a glassy carbon disk (4 mm diameter) was employed as the working electrode. A Pt-foil and a saturated calomel reference electrode were used as the auxiliary and reference electrode, respectively. Cyclic voltammetry (CV) experiments were carried out at 25 °C in 0.5 M H_2SO_4 solution. About 5 mg of catalyst was ultrasonically suspended with 2 mL of ethanol and 50 μL of 5 wt % Nafion solution for 15 min, and then about 10 μL of suspension was spread on the clean glass carbon electrode and dried to obtain a thin active layer. Before each measurement, fast potential pulses (100 mV s^{-1}) between 0 and 1400 mV were applied to the electrodes for surface cleaning and for obtaining a reproductive active electrochemical surface. The electrochemical surface area (ECSA) of the Pt−Mo_2C/CNTs catalyst was determined by integrating the hydrogen adsorption/desorption areas of the cyclic voltammogram. The potential was then cycled at 25 mV s^{-1} starting at −0.24 V for two complete oxidation/reduction cycles.

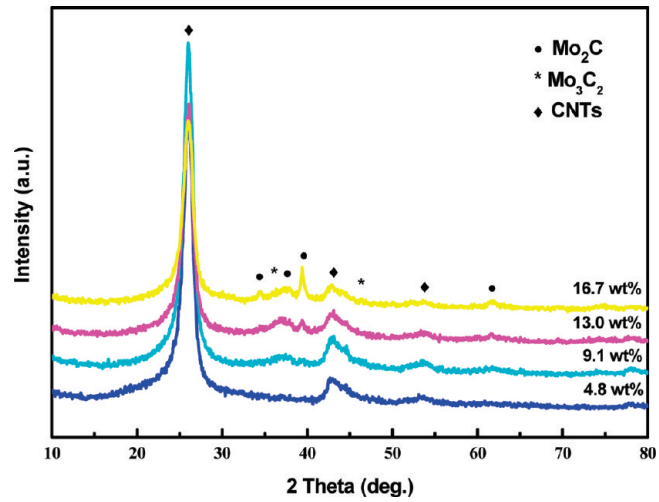

Figure 1. XRD patterns of the Mo_2C/CNTs samples with different Mo loading from the microwave-assisted thermolytic molecular precursor method.

The activity of ORR on these catalysts was evaluated on the thin-film rotating disk electrode (Pine Instruments, USA). For the thin-film rotating disk electrode measurements, 10 μL of the well-dispersed catalyst ink, which was prepared in the CV test, was spread onto the clean glass carbon disk, as described in CV tests. ORR activity was measured in oxygen-saturated 0.5 M H_2SO_4 electrolyte at 25 ± 0.5 °C with a CHI 6DOC potentiostat/galvanostat. A linear sweep was started from the cathodic direction at a scan rate of 5 mV s^{-1}, and the rotating speed was fixed at 1600 rpm. The electrolyte was bubbled with an oxygen flow for about 1 h before each experiment and maintained over the electrolyte during the whole voltammetry measurement.

3. Results and Discussion

The Mo_xC/CNTs samples with 4.8, 9.1, 13.0, and 16.7 wt % Mo calculated loading were prepared by microwave-assisted thermolytic molecular precursor method. XRD patterns of the obtained samples with 15 min microwave irradiation were shown in Figure 1. No diffraction peaks assigned to $Mo(CO)_6$ were observed for all of the samples, indicating the precursors have decomposed thoroughly. The diffraction peaks at 26.5°, 43.8°, and 54.0° observed in the diffraction of CNTs can be attributed to the hexagonal graphite structure. No distinct peaks attributed to Mo_xC phase were detected for the 4.8 wt % samples, suggesting the highly dispersed Mo_xC on CNTs. The XRD pattern of the 13.0 wt % sample showed a diffraction peak at 39.4°, which is due to β-Mo_2C with a hexagonal closed

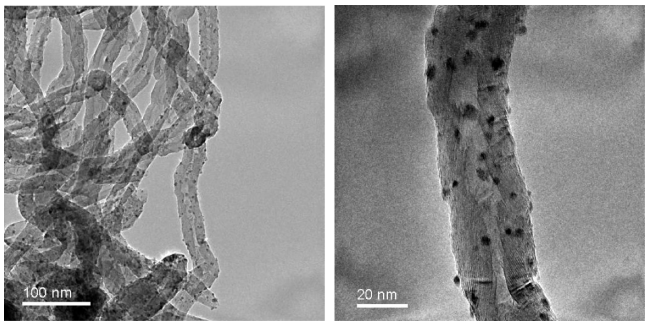

Figure 2. TEM images of the Mo_2C/CNTs sample with the 16.7 wt % Mo calculated loading.

packed structure. The XRD patterns of the 13.0 wt % samples showed three typical diffraction peaks at 37.9°, 39.4°, and 61.5°, which were, respectively, assigned to the (002), (101), and (110) crystal face of β-Mo_2C with hexagonal closed-packed structure. Further increasing the Mo loading to 16.7 wt %, the diffraction peaks became sharper, which could be ascribed to the growth of Mo_2C. The average particle sizes of β-Mo_2C estimated from the parameters of XRD according to the Scherrer formula are 3.6 and 6.2 nm for the 13.0 and 16.7 wt % samples, respectively. The result is consistent with that obtained in Mo/HSAC by carbothermal hydrogen reduction method, in which the particle sizes of β-Mo_2C also increased with increasing Mo loading.[35] Simultaneously, weak diffraction peaks due to Mo_3C_2 also were observed on the Mo_xC/CNTs samples with 13.0 and 16.7 wt % Mo calculated loading, which were not found in the temperature-programmed methods.[34] Formation of the Mo_3C_2 phase in the samples with relatively high Mo loading was proposed from the Mo_2C conversion at the high temperature under the microwave irradiation.

The particle sizes of the Mo_2C/CNTs sample are confirmed by using the TEM measurements. The typical TEM images of the Mo_2C/CNTs sample with the 16.7 wt % Mo calculated loading undergoing 15 min of microwave irradiation were shown in Figure 2. Nanostructured Mo_2C particles were well distributed on the outer surface of CNTs, and no agglomerations were observed. The mean size of Mo_2C particles was about 5 nm, which is in good agreement with the value from XRD. This further confirmed that the microwave-assisted thermolytic molecular precursor method was an efficient way for the synthesis of evenly monodispersed molybdenum carbides with nanostructure.

To obtain the actual molybdenum loading, TG experiments were carried out in air. In the oxidation process, Mo_2C in the Mo_2C/CNTs was supposed to convert completely into MoO_3, and CNTs were oxidized into CO_2 or CO. The Mo loading (x %) can be calculated by the formula:

$$x\,\% = \frac{m_1}{m_0}\frac{M_{\mathrm{Mo}}}{M_{\mathrm{MoO_3}}} \times 100\%$$

where m_0 and m_1 are the masses of the Mo_2C/CNTs sample and the final products, respectively, and M_{MoO3} and M_{Mo} are the molecular masses of MoO_3 and Mo, respectively. As shown in Figure 3, the TG curves of the Mo_2C/CNTs samples with the 16.7 and 9.1 wt % calculated Mo loading showed the gradually increase in weight from 50 to 485 °C, indicating the occurrence of Mo_2C oxidation to MoO_3. The rapid loss of the weight from 485 to 600 °C was attributed to the oxidation of CNTs to CO_2 or CO. From the TG data, the actual Mo loading was 6.8 and 13.8 wt %, respectively, which is lower

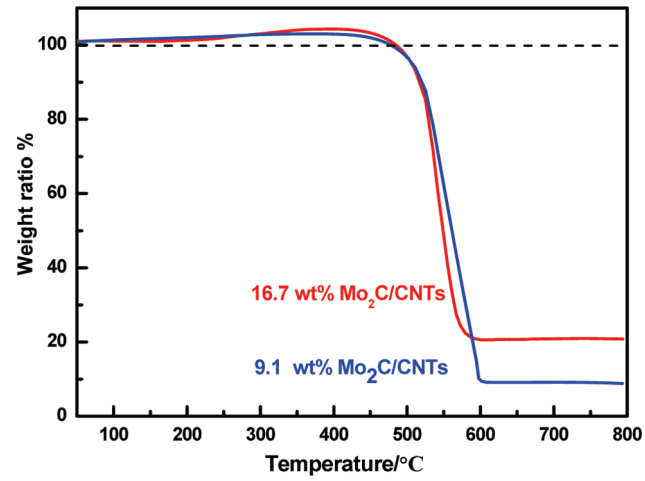

Figure 3. TG curves of the Mo_2C/CNTs samples with 9.1 and 16.7 wt % Mo calculated loadings.

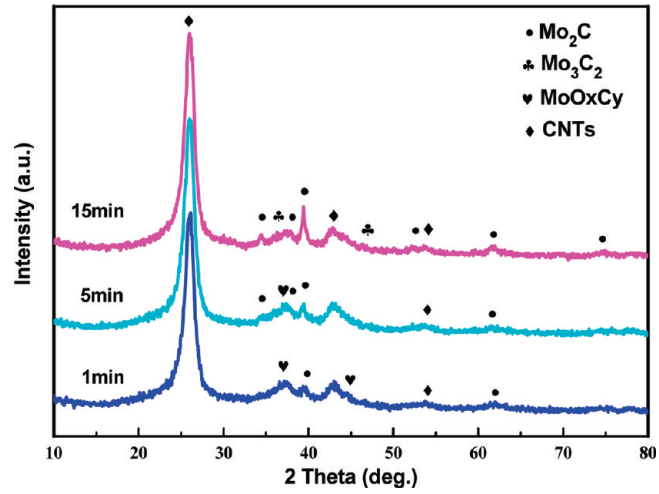

Figure 4. XRD patterns of the Mo_xC/CNTs samples with different reaction time.

than the Mo calculated loading 9.1 and 16.7 wt %. This loss in loading may be due to the evaporation of the intermediates (i.e., Mo, MoO_xC_y) during the formation process.

To understand the formation mechanism of nanostructured Mo_2C on CNTs, the preparation was monitored with different microwave irradiation time. The XRD patterns of the samples with the 16.7 wt % Mo calculated loading from 1, 5, and 15 min microwave irradiation were shown in Figure 4. After 1 min of microwave irradiation, two clear diffraction peaks at 37.3° and 44.6° due to the MoO_xC_y phase appeared, while a weak peak at 19.4° due to Mo_2C also emerged. This was attributed to precipitation of O inside the MoO_xC_y and carburization of external surface of MoO_xC_y particles.[22–24] With increasing reaction time to 5 min, the diffraction peaks due to MoO_xC_y phase became weak, and those due to Mo_2C became sharper. Meanwhile, diffraction peaks at 36.4° and 46.4° assigned to Mo_3C_2 phase appeared. Further increasing the reaction time to 15 min, the diffraction peaks due to Mo_2C became much sharper, while the diffraction peaks due to Mo_3C_2 phase also became clear. It was found that the inner wall of the reactor was covered by a layer of metallic Mo when the microwave irradiation time was 0.5 min. This was due to the decomposition of $Mo(CO)_6$ precursor to metallic Mo in the initial step, which is in agreement with conservations in literature.[41] With the increase of microwave irradiation time, the MoO_xC_y phase first was formed by

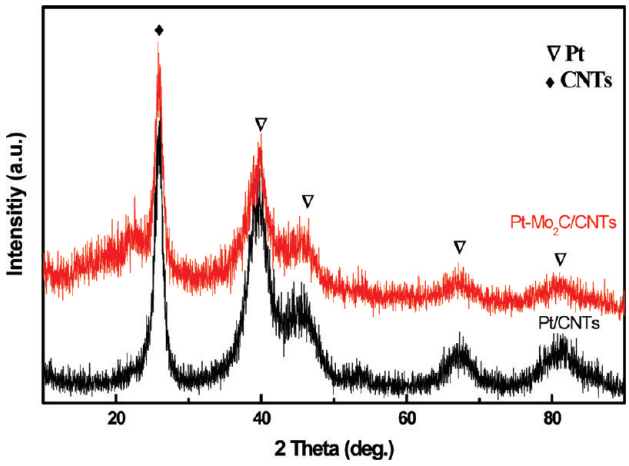

Figure 5. XRD patterns of the 18.3 wt % Pt/CNTs and 16.0 wt % Pt−Mo_2C/CNTs samples.

the reaction between metallic Mo and active carbon species from CO. The MoO_xC_y phase was further carburized to Mo_2C with the increase of microwave irradiation time. CO had been used as the carbon source to carburize tungsten oxides to obtained tungsten carbides.[42] They found that carburization in pure CO always resulted in the deposition of free carbon (C*) on the surface of the carbides, and the amount of free carbon was correlated with the progress from W_2C to WC. Accordingly, the reaction scheme of the molybdenum carbide formation can be postulated as follows:

$$Mo(CO)_6 \rightarrow Mo + 6CO$$

$$2CO \rightarrow C^* + CO_2$$

$$Mo + xCO \rightarrow MoO_xC_y + (x-y)C^*$$

$$2MoO_xC_y + (2x - 2y + 1)C^* \rightarrow Mo_2C + 2xCO$$

$$3Mo_2C + C^* \rightarrow 2Mo_3C_2$$

$$3Mo_2C + 2CO \rightarrow 2Mo_3C_2 + CO_2$$

The above-mentioned reactions were further confirmed by the analysis of gaseous products, which included CO_2 and CO. The $Mo(CO)_6$ precursor was first decomposed to form Mo and CO, and then the CO dismutation reaction occurred. Next, the metallic Mo was converted to MoO_xC_y and free carbon by the reaction with CO. The MoO_xC_y phase was further carburized to Mo_2C by the free carbon or CO. Also, Mo_2C would be further transformed into Mo_3C_2 by carburization of free carbon or CO. Further study is in progress to understand the detailed formation mechanism of the molybdenum carbides in the microwave-assisted thermolytic molecular precursor method.

The Pt−Mo_2C/CNTs and Pt/CNTs samples were prepared by the modified ethylene glycol method. The Pt contents from ICP-OES of Pt/CNTs and Pt−Mo_2C/CNTs samples were 18.3 and 16.0 wt %, respectively. Their XRD patterns were shown in Figure 5. For the two samples, the diffraction peaks at 39.67°, 46.17°, 67.40°, and 81.23° were detected and could be attributed to the (111), (200), (220), and (311) crystal face of metallic Pt with face-centered cubic crystalline structure, while the diffraction peaks at 26.5° and 43.5° were ascribed to graphite with hexagonal structures. It is difficult to distinguish the diffraction peaks of Pt and Mo_2C in the XRD patterns due to the tiny difference in crystal lattice spacing. The average particle size of Pt estimated from the Pt (111) peak with the Scherrer equation was approximately 3.5 nm in the Pt−Mo_2C/CNTs sample.

As observed in a typical TEM image of Pt−Mo_2C/CNTs sample (Figure 6), all of the particles were of sphere shape, and no agglomerations were detected. The particle size varied from 3 to 6 nm, which was in good agreement with the results obtained from the XRD. The HRTEM image in Figure 6 showed that the Pt particles obtained through the reduction of ethylene glycol method were more likely to be closed with or in conglutination with the Mo_2C particles, which was quite different from the Pt−WC_x/CNTs samples gained through the same way.[34]

The homogeneous Mo_2C and Pt distributions in the Pt−Mo_2C/CNTs sample were also confirmed by the STEM dark field image, and the corresponding elemental maps were shown in Figure 7. The outer wall of the CNTs was uniformly covered by well-dispersed molybdenum carbides and Pt without agglomeration.

Cyclic voltammograms of the 18.3 wt % Pt/CNTs and 16.0% Pt−Mo_2C/CNTs samples in 0.5 M H_2SO_4 solution at a scan rate of 25 mV s^{-1} were presented in Figure 8. The Pt/CNTs catalyst showed two pairs of hydrogen adsorption/desorption peaks, typically characteristics of polycrystalline Pt.[43] The Pt−Mo_2C/CNTs catalyst exhibited symmetric hydrogen adsorption/desorption currents in the low potential region, indicating surface properties quite different from those of Pt/CNTs. The ECSA of the Pt−Mo_2C/CNTs and Pt/CNTs catalysts was determined by integrating the hydrogen adsorption/desorption areas of the cyclic voltammogram obtained in a potential pulse at a scan rate of 25 mV s^{-1}. Obviously, Pt−Mo_2C/CNTs possessed a higher ECSA than Pt/CNTs, which could be attributed to the unique nanostructured Mo_2C/CNTs and well-dispersed Pt nanoparticles with the sizes of 3−6 nm on the surface of Mo_2C/CNTs.

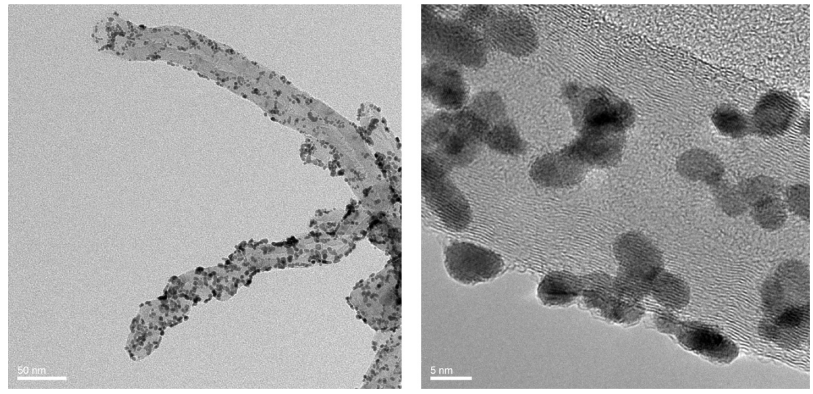

Figure 6. TEM (left) and HRTEM (right) images of the 16.0 wt % Pt−Mo_2C/CNTs sample.

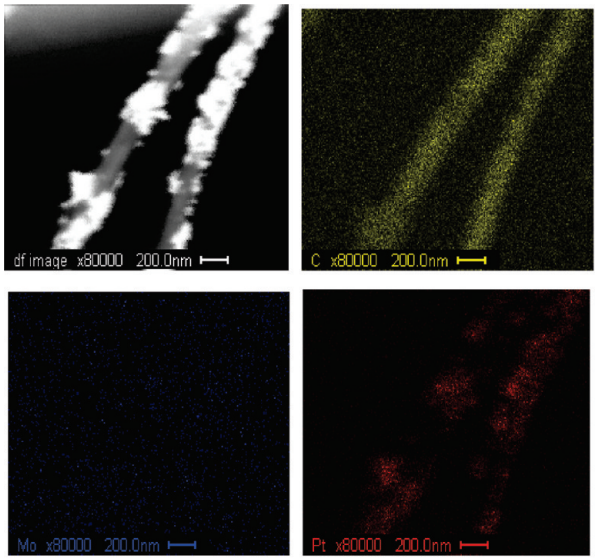

Figure 7. Representative STEM dark-field images and corresponding elemental maps of Pt (red), C (yellow), and Mo (blue) for the 16.0 wt % Pt−Mo_2C/CNTs sample.

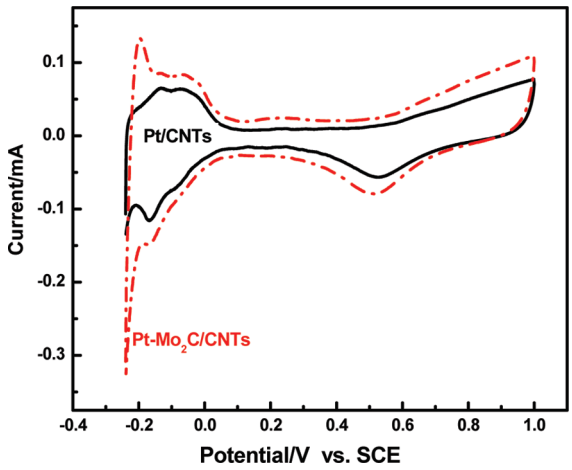

Figure 8. Cyclic voltammograms of the 18.3 wt % Pt/CNTs and 16.0 wt % Pt−Mo_2C/CNTs catalysts in a solution of 0.5 M H_2SO_4 with the scan rate of 50 mV/s at 25 °C.

Figure 9 showed the linear sweep voltammograms of the CNTs, 16.7 wt % Mo_2C/CNTs, 18.3 wt % Pt/CNTs, and 16.0 wt % Pt−Mo_2C/CNTs samples in the O_2-saturated 0.5 M H_2SO_4 solution. CNTs sample did not show electrocatalytic activity toward ORR in acid solution, while the Mo_2C/CNTs catalyst somewhat had electrocatalytic activity, although its overpotential was slightly larger than those of other catalysts. Both the Pt−Mo_2C/CNTs and the Pt/CNTs catalysts represented high electrocatalytic activity toward ORR. The 16.0 wt % Pt−Mo_2C/CNTs catalyst had a more positive onset potential of 85 mV as compared to the 18.3 wt % Pt/CNTs catalyst, which could be attributed to a synergistic effect among Pt, Mo_2C, and CNTs. Additionally, because the Mo_2C particles had occupied part of the reaction sites on CNTs, a few Pt particles had nowhere to stay, and the actual Pt loading of Pt/CNTs sample was a little larger than that of Pt−Mo_2C/CNTs as shown in the ICP-OES measurement. It could be supposed that the Pt−Mo_2C/CNTs would surpass Pt/CNTs more in electrocatalytic activity toward ORR with the same Pt loading. This performance implied that Mo_2C/CNTs was an efficient support for electrocatalyst and possessed a good ability in cutting down the Pt usage.

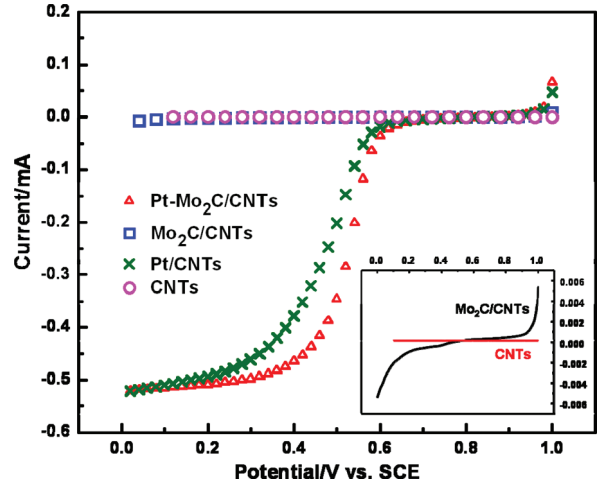

Figure 9. The linear sweeping curves of O_2 at CNTs, Mo_2C/CNTs, 18.3 wt % Pt/CNTs, and 16.0 wt % Pt−Mo_2C/CNTs in a solution of 0.5 M H_2SO_4 with a scan rate of 5 mV/s at 25 °C (inset: the magnified image of the linear sweeping curves of O_2 at CNTs and Mo_2C/CNTs).

4. Conclusion

Sphere-like Mo_2C particles with 3−6 nm had been successfully synthesized and well distributed on CNTs by the microwave-assisted thermolytic molecular precursor method. The formation of Mo_2C includes the following steps: decomposition of $Mo(CO)_6$ precursor to the metallic Mo and CO, CO dismutation reaction, formation of the MoO_xC_y by the metallic Mo and CO, the MoO_xC_y carburization to Mo_2C, and reaction of Mo_2C to Mo_3C_2. The Pt−Mo_2C/CNTs sample prepared by the modified ethylene glycol method showed evenly monodispersed Pt particles with 3−6 nm. The Pt−Mo_2C/CNTs gave higher electrochemical surface area and ORR activity with a more positive onset potential in acid solution than those of Pt/CNTs under the same condition, which was attributed to the synergistic effect among Pt, Mo_2C, and CNTs. The findings indicate that Mo_2C is an inexpensive and promising alternative to precious metal and worthy of further exploring for other applications in catalysis.

Acknowledgment

We gratefully acknowledge the financial support provided by the Scientific and Technical Foundation of Educational Committee of Liaoning Province, Foundation for Returness of Ministry of Education of China, and the State Key Laboratory of Fine Chemicals.

Literature Cited

(1) Thomas, S. C.; Ren, X. M.; Gottesfeld, S.; Zelenay, P. Direct Methanol Fuel Cells: Progress in Cell Performance and Cathode Research. *Electrochim. Acta* **2002**, *47*, 3741.

(2) Shukla, A. K.; Christensen, P. A.; Dickinson, A. J.; Hamnett, A. A Liquid-feed Solid Polymer Electrolyte Direct Methanol Fuel Cell Operating at Near-ambient Conditions. *J. Power Sources* **1998**, *76*, 54.

(3) Tarasevich, M. R.; Sadkowski, A.; Yeager, E. In *Comprehensive Treatise of Electrochemistry*; Conway, B. E., Bockris, J. O. M., Yeager, E., Khan, S. U. M., White, R. E., Eds.; Plenum Press: New York, 1983; Vol. 7, p 301.

(4) Adzic, R. R. In *Electrocatalysis*; Lipkowski, J., Ross, P. N., Eds.; Wiley: New York, 1998; p 197.

(5) Gasteiger, H. A.; Kocha, S. S.; Sompalli, B.; Wagner, F. T. Activity Benchmarks and Requirements for Pt, Pt-alloy, and Non-Pt Oxygen Reduction Catalysts for PEMFCs. *Appl. Catal., B* **2005**, *56*, 9.

(6) Shao, Y. Y.; Liu, J.; Wang, Y.; Lin, Y. H. Novel Catalyst Support Materials for PEM Fuel Cells: Current Status and Future Prospects. *J. Mater. Chem.* **2009**, *19*, 46.

(7) Bessel, C. A.; Laubernds, K.; Rodriguez, N. M.; Baker, R. T. K. Graphite Nanofibers as an Electrode for Fuel Cell Applications. *J. Phys. Chem. B* **2001**, *105*, 1115.

(8) Joo, S. H.; Choi, S. J.; Oh, I.; Kwak, J.; Liu, Z.; Terasaki, O.; Ryoo, R. Ordered Nanoporous Arrays of Carbon Supporting High Dispersions of Platinum Nanoparticles. *Nature* **2001**, *412*, 169.

(9) Zhong, H. X.; Zhang, H. M.; Liu, G.; Liang, Y. M.; Hu, J. W.; Yi, B. L. A Novel Non-noble Electrocatalyst for PEM Fuel Cell Based on Molybdenum Nitride. *Electrochem. Commun.* **2006**, *8*, 707.

(10) Jeon, M. K.; Daimon, H.; Lee, K. R.; Nakahara, A.; Woo, S. I. CO Tolerant Pt/WC Methanol Electro-oxidation Catalyst. *Electrochem. Commun.* **2007**, *9*, 2692.

(11) Nie, M.; Shen, P. K.; Wei, Z. D. Nanocrystaline Tungsten Carbide Supported Au-Pd Electrocatalyst for Oxygen Reduction. *J. Power Sources* **2007**, *167*, 69.

(12) Ganesan, R.; Lee, J. S. Tungsten Carbide Microspheres as a Noble-metal-economic Electrocatalyst for Methanol Oxidation. *Angew. Chem., Int. Ed.* **2005**, *44*, 6557.

(13) Chen, J. G. G. Carbide and Nitride Overlayers on Early Transition Metal Surfaces: Preparation, Characterization, and Reactivities. *Chem. Rev.* **1996**, *96*, 1477.

(14) Hwu, H. H.; Chen, J. G. G. Surface Chemistry of Transition Metal Carbides. *Chem. Rev.* **2005**, *105*, 185.

(15) Lang, H.; Blau, S.; Rheinwald, G.; Wildermuth, G. Pyrolyse von Übergangsmetallkomplexen: Darstellung von Metallcarbiden (MC, M_2C) aus Metallorganischen Verbindungen. *J. Organomet. Chem.* **1995**, *489*, C17.

(16) Chouzier, S.; Afanasiev, P.; Vrinat, M.; Cseri, T.; Roy-Auberger, M. One-step Synthesis of Dispersed Bimetallic Carbides and Nitrides from Transition Metals Hexamethylenetetramine Complexes. *J. Solid State Chem.* **2006**, *179*, 3314.

(17) Pol, S. V.; Pol, V. G.; Gedanken, A. Synthesis of WC Nanotubes. *Adv. Mater.* **2006**, *18*, 2023.

(18) Nelson, J. A.; Wagner, M. J. High Surface Area Mo_2C and WC Prepared by Alkalide Reduction. *Chem. Mater.* **2002**, *14*, 1639.

(19) Li, C.; Yang, X. G.; Yang, B. J.; Qian, Y. T. A Chemical Co-Reduction Route to Synthesize Nanocrystalline Vanadium Carbide. *J. Am. Ceram. Soc.* **2006**, *89*, 320.

(20) Volpe, L.; Bourdart, M. Compounds of Molybdenum and Tungsten with High Specific Surface Area: II. Carbides. *J. Solid State Chem.* **1985**, *59*, 348.

(21) Lee, J. S.; Oyama, S. T.; Bourdart, M. Molybdenum Carbide Catalysts: I. Synthesis of Unsupported Powders. *J. Catal.* **1987**, *106*, 125.

(22) Mordenti, D.; Brodzki, D.; Djéga-Mariadassou, G. New Synthesis of Mo_2C 14 nm in Average Size Supported on a High Specific Surface Area Carbon Material. *J. Solid State Chem.* **1998**, *141*, 114.

(23) Liang, C. H.; Ying, P. L.; Li, C. Nanostructured β-Mo_2C Prepared by Carbothermal Hydrogen Reduction on Ultrahigh Surface Area Carbon Material. *Chem. Mater.* **2002**, *14*, 3148.

(24) Liang, C. H.; Tian, F. P.; Li, Z. L.; Feng, Z. C.; Wei, Z. B.; Li, C. Preparation and Adsorption Properties for Thiophene of Nanostructured W_2C on Ultrahigh-Surface-Area Carbon Materials. *Chem. Mater.* **2003**, *15*, 4846.

(25) Mdleleni, M. M.; Hyeon, T.; Suslick, K. S. Sonochemical Synthesis of Nanostructured Molybdenum Sulfide. *J. Am. Chem. Soc.* **1998**, *120*, 6189.

(26) Dantsin, G.; Suslick, K. S. Sonochemical Preparation of a Nanostructured Bifunctional Catalyst. *J. Am. Chem. Soc.* **2000**, *122*, 5214.

(27) Nikitenko, S. I.; Koltypin, Y.; Palchik, O.; Felner, I.; Xu, X. N.; Gedanken, A. Synthesis of Highly Magnetic, Air-Stable Iron Carbide Nanocrystalline Particles by Using Power Ultrasound. *Angew. Chem., Int. Ed.* **2001**, *40*, 4447.

(28) Loupy, A. *Microwaves in Organic Synthesis*; Wiley-VCH: Weinheim, 2002; p 345.

(29) Tompsett, G. A.; Conner, W. C.; Yngvesson, K. S. Microwave Synthesis of Nanoporous Materials. *ChemPhysChem* **2006**, *7*, 296.

(30) Vallance, S. R.; Kingman, S.; Gregory, D. H. Ultrarapid Materials Processing: Synthesis of Tungsten Carbide on Subminute Timescales. *Adv. Mater.* **2007**, *19*, 138.

(31) Vallance, S. R.; Kingman, S.; Gregory, D. H. Ultra-Rapid Processing of Refractory Carbides; 20s Synthesis of Molybdenum Carbide, Mo_2C. *Chem. Commun.* **2007**, 742.

(32) Hu, F. P.; Cui, G. F.; Wei, Z. D.; Shen, P. K. Improved Kinetics of Ethanol Oxidation on Pd Catalysts Supported on Tungsten Carbides/Carbon Nanotubes. *Electrochem. Commun.* **2008**, *10*, 1303.

(33) Bender, J.; Dunn, J.; Brezinsky, K. In *Catalyst Preparation: Science and Engineering*; Regalbuto, J., Ed.; CRC Press: New York, 2007; Vol. 7, p 141.

(34) Serp, P.; Kalck, P.; Feurer, R. Chemical Vapor Deposition Methods for the Controlled Preparation of Supported Catalytic Materials. *Chem. Rev.* **2002**, *102*, 3085.

(35) Liang, C. H.; Xia, W.; Soltani-Ahmadi, H.; Schlüter, O.; Fischer, R. A.; Muhler, M. The Two-Step Chemical Vapor Deposition of Pd(allyl)Cp as an Atom-Efficient Route to Synthesize Highly Dispersed Palladium Nanoparticles on Carbon Nanofibers. *Chem. Commun.* **2005**, 282.

(36) Liang, C. H.; Ding, L.; Wang, A. Q.; Ma, Z. Q.; Qiu, J. S.; Zhang, T. Microwave-Assisted Preparation and Hydrazine Decomposition Properties of Nanostructured Tungsten Carbides on Carbon Nanotubes. *Ind. Eng. Chem. Res.* **2009**, *48*, 3244.

(37) Ding, L. Microwave-assisted Preparation of Transition Metal Carbides and Their Catalytic Properties. M.S. Thesis, Dalian University of Technology, 2009.

(38) Li, W. Z.; Liang, C. H.; Zhou, W. J.; Qiu, J. S.; Zhou, Z. H.; Sun, G. Q.; Xin, Q. Preparation and Characterization of Multiwalled Carbon Nanotube-supported Platinum for Cathode Catalysts of Direct Methanol Fuel Cells. *J. Phys. Chem. B* **2003**, *107*, 6292.

(39) Li, W. Z.; Liang, C. H.; Zhou, W. J.; Qiu, J. S.; Li, H. Q.; Sun, G. Q.; Xin, Q. Homogeneous and Controllable Pt Particles Deposited on Multi-wall Carbon Nanotubes as Cathode Catalyst for Direct Methanol Fuel Cells. *Carbon* **2004**, *42*, 436.

(40) Li, W. Z.; Liang, C. H.; Zhou, W. J.; Qiu, J. S.; Han, H. M.; Wei, Z. B.; Sun, G. Q.; Xin, Q. Carbon Nanotubes as Support for Cathode Catalyst of a Direct Methanol Fuel Cell. *Carbon* **2002**, *40*, 791.

(41) Chen, H. Y.; Chen, L.; Lu, L.; Hong, Q.; Chua, H. C.; Tang, S. B.; Lin, J. Synthesis, Characterization and Application of Nano-structured Mo_2C Thin Films. *Catal. Today* **2004**, *96*, 161.

(42) Lemaitre, J.; Vidick, B.; Delmon, B. Control of the Catalytic Activity of Tungsten Carbides: I. Preparation of Highly Dispersed Tungsten Carbides. *J. Catal.* **1986**, *99*, 415.

(43) Bard, A. J.; Faulkner, L. R. *Electrochemical Method, Fundamentals and Application*; Wiley: New York, 1980.

Received for review November 3, 2009
Revised manuscript received March 7, 2010
Accepted March 14, 2010

IE901741C